The Development of Dynamic CFD Model of the Magnetic Semi-Levitation of Liquid Metals

K.Pericleous, V.Bojarevics, M.Cross, and G.Tinios

University of Greenwich, Wellington Str., London SE18 6PF, UK

ABSTRACT

In the casting of reactive metals, such as titanium alloys, contamination can be prevented if there is no contact between the hot liquid metal and a solid crucible. This can be achieved by containing the liquid metal by means of high frequency AC magnetic field. A water cooled current-carrying coil, surrounding the metal can then provide the required Lorentz forces, and at the same time the current induced in the metal can provide the heating required to melt it.

This 'attractive' processing solution has however many problems, the most serious being that of the control and containment of the liquid metal envelope, which requires a balance of the gravity and induced inertia forces on the one side, and the containing Lorentz and surface tension forces on the other. To model this process requires a fully coupled dynamic solution of the flow field, magnetic field and heat transfer/melting process to account for. A simplified solution has been published previously (Bhamidipati & El-Kaddah 1991) providing quasi-static solutions only, by taking the irrotational 'magnetic pressure' term of the Lorentz force into account. The authors remedy this deficiency by modelling the full problem using CFD techniques. The salient features of these techniques are included in this paper, as space allows.

Keywords: Magneto-Hydrodynamics, Electromagnetic Casting, Metals Processing.

NOMENCLATURE

- $\mathbf{A}$ Electromagnetic vector potential
- $\mathbf{B}$ Magnetic field
- C_p Specific heat
- g gravity
- h experimental heat transfer coefficient
- I_s current in the coil
- $\mathbf{J}$ electric current density
- K mean curvature
- K_D Darcy coefficient
- l_m turbulent mixing length
- M electromagnetic mutual inductance
- $\mathbf{n}$ normal
- p pressure
- P_n Legendre function
- q_l latent heat
- R radial spherical co-ordinate
- $\mathbf{R}$ radius vector
- R_0 radius for reference sphere
- s shape function
- t time
- T temperature
- T_w wall temperature
- u_{nmk} spectral expansion coefficients
- $\mathbf{v}$ velocity
- $\mathbf{w}$ vorticity
- Z cylindrical co-ordinate
- α_e effective thermal diffusivity
- γ surface tension coefficient
- φ azimuthal co-ordinate
- μ transformed co-ordinate
- μ_0 magnetic permeability
- ν kinematic viscosity
- ν_e effective kinematic viscosity
- θ spherical co-ordinate
- ρ density
- σ electrical conductivity
- τ surface tangent
- ω AC frequency

INTRODUCTION

Metals can be melted, confined and supported by means of a high frequency magnetic field generated by external coils of complex configuration. For high purity and reactive metal alloys, like titanium aluminides, contact with refractory material crucibles must be avoided. Magnetic levitation melting is a well known method for this purpose; yet it suffers from disadvantages due to a limit on the mass levitated and various instabilities. The cold crucible technique is actually used for this type of melt, offering all the advantages of electromagnetic liquid metal processing and avoiding the crucible wall contact with the liquid metal. However, the water-cooled crucible sections make the process inherently of low energy efficiency. A compromise between the levitation and cold crucible methods is known as magnetic semi-levitation or suspension melting (Bhamidipati & El-Kaddah 1991) which uses a water cooled annular chill block merely at the basis of the metal charge to be melted. Initially a solid cylindrical billet is placed on the chill block, and a coaxial AC coil is gradually moved downwards as the metal is being melted, confined and stirred owing to the induced electric current and the magnetic field. Finally the melting front reaches the bottom and the liquid metal fills a mould through the central hole in the chill block. A detailed description of the process can be found in (Bhamidipati 1995).

The magnetic field at the boundary of liquid metal can be viewed as a superposition of the external field supplied by the fixed AC coil and an oppositely directed field generated by current induced in the metal, which gives a skin layer penetration effect for the external electromagnetic field of a high frequency. In the case of pure levitation melting, relatively high frequencies are typically used (10^4-10^5 Hz), which justifies the use of different electromagnetic skin-layer based theories (Sneyd&Moffatt 1982, Mestel 1982). However, a typical frequency used in the semi-levitation melting process is an order of magnitude lower and the magnetic field penetration is significant (approximately 10% of the charge radius in the computed example case, see Fig. 1). Moreover, top turn(s) of the source coil are usually carrying oppositely directed "stabilising" current, which leads to a zero tangential magnetic field at a neutral point on the free surface of liquid metal. The region at this neutral point can be a new source of instabilities for some coil designs, since no magnetic holding force is exerted at the neutral point. The magnetic field lines of the current induced in the metal are closing within the internal part of the liquid, and the resulting electromagnetic force is rotational, in general, generating an additional fluid motion. Yet the most important fluid motion is created because of the dynamic external boundary shaping: when the metal is being melted, the magnetic confining force pushes the liquid radially inwards to the symmetry axis and upwards until a balance with gravity force is reached. With inertial effects this can lead to an oscillating interface motion and waves, the damping of which depends on the effective turbulent viscosity. In addition to the fluid flow and electromagnetic field coupling with the liquid metal shape change, there is a coupling to the temperature field (Joule heat generation, heat transfer, melting front motion, and the temperature dependence of material properties).

The CFD approach presented here is based on a continuous co-ordinate transformation method which maps the deforming boundary to a sphere. The transformed governing equations and boundary conditions are solved by a spectral collocation method which permits resolution of the highly non-linear mathematical problem. The electromagnetic field numerical solution is obtained by a volume integral method that determines the solution in the liquid metal region with a high resolution in the boundary layer. The results presented here will demonstrate the complex fluid motion and the interdependence of the heat, momentum and electromagnetic fields in this problem.

PROBLEM STATEMENT AND SOLUTION

To a good approximation the semi-levitation problem can be considered as axisymmetric. Let us consider an axisymmetric volume of metal which initially is solid and is gradually being melted. The governing equations for the

turbulent flow and heat transfer can be represented in the following form:

$$\begin{aligned}
&\partial_t \mathbf{v} - \mathbf{v}\times\mathbf{w} = -\nabla(\rho^{-1}p + \tfrac{1}{2}\mathbf{v}^2)\\
&+\nabla\cdot(\nu_e(\nabla\mathbf{v}+\nabla\mathbf{v}^*)) - K_D\mathbf{v}\\
&+\rho^{-1}\mathbf{j}\times\mathbf{B} + \mathbf{g},\\
&\nabla\cdot\mathbf{v} = 0,\\
&\partial_t T + \mathbf{v}\cdot\nabla T = \nabla\cdot(\alpha_e\nabla T)\\
&+(\rho C_p)^{-1}(j^2/\sigma + q_l),
\end{aligned} \tag{1}$$

where $\mathbf{v}$ is the velocity vector, p the pressure, ρ the density, $\mathbf{w} = \nabla\times\mathbf{v}$ the vorticity, $\nu_e(\nabla\mathbf{v}+\nabla\mathbf{v}^*)$ is the effective turbulent viscosity with the velocity deformation rate tensor in dyadic representation, $-K_D\mathbf{v}$ is Darcy term for mushy zone and melting front modelling, $\mathbf{j}\times\mathbf{B}$ is electromagnetic force, $\mathbf{g}$ gravity, T temperature, α_e effective turbulent thermal diffusivity, C_p specific heat, j^2/σ Joule heat, and q_l latent heat. There can be two types of boundary conditions for velocities at different portions (in general) of the external boundary:

1. at solid walls (no slip for velocities)

$$u_n = 0, u_\tau = 0 \tag{2}$$

2. free boundary (normal stress = surface tension, no tangential stress, kinematic condition)

$$\Pi_{nn} = \gamma K \ , \ \Pi_{n\tau} = 0 \ , \tag{3a}$$

$$V_R = \partial_t R + \mathbf{v}\cdot\nabla\mathbf{R} \quad (\mathbf{R} = \mathbf{e}_\mathbf{R} R(\theta,t)) \tag{3b}$$

For temperature at boundaries we adopt an effective heat transfer given by experimentally determined heat transfer coefficient $h(T)$ (Bhamidipati 1995):

$$-\rho C_p \alpha_e \partial_n T = h(T - T_w), \tag{4}$$

where T_w is wall or ambient air temperature. The effective thermal diffusivity and viscosity are represented as sums of molecular and turbulent diffusivities. The turbulent thermal diffusivity is assumed to be equal to the turbulent viscosity ν_T which is computed according to a generalised mixing length hypothesis:

$$\begin{aligned}
&\nu_T = l_m^2 \tfrac{1}{2}\sqrt{[(\nabla\mathbf{v}+\nabla\mathbf{v}^*):(\nabla\mathbf{v}+\nabla\mathbf{v}^*)]},\\
&l_m = f_l \frac{|\mathbf{v}|}{\tfrac{1}{2}\sqrt{[(\nabla\mathbf{v}+\nabla\mathbf{v}^*):(\nabla\mathbf{v}+\nabla\mathbf{v}^*)]}+|\mathbf{v}|/R_0}
\end{aligned} \tag{5}$$

where the mixing length l_m is expressed by dimensional considerations, $f_l = 1$ in the present calculations. This model for the turbulent viscosity was found to be the most satisfactory between other variants of mixing length expressions commonly used for the engineering simulations, and it is assumed to be effective for recirculating flows with free boundaries, i.e. in cases where no satisfactory turbulent viscosity models are generally accepted.

The initial shape is cylindrical, however, we prefer to use spherical polar coordinates because during the melting process the boundary of liquid metal can assume shapes which are more easily described as deformed spheres. The spherical coordinates (R, θ), with the origin in the middle of the melted body, are transformed to computationally convenient new coordinates:

$\bar{R} = R_0^{-1}(1 + s(\mu,t))^{-1}R$, $\mu = \cos\theta$, $\bar{t} = t$,

where the continuous function $s(\mu,t)$ depends on polar angle and time, R_0 is a reference sphere radius. The equations and boundary conditions (1)-(5) are first expressed in spherical coordinates and then transformed to the new coordinates with the appropriate expressions for the derivatives, e.g.,

$$\begin{aligned}
&\partial_R \mathrm{v} = \frac{1}{\mathrm{R}_0(1+s)}\partial_{\bar{R}}\mathrm{v},\\
&\partial_\theta \mathrm{v} = -\sqrt{1-\mu^2}\,(\partial_\mu \mathrm{v} - \frac{\bar{R}\partial_\mu s}{1+s}\partial_{\bar{R}}\mathrm{v}),\\
&\partial_t \mathrm{v} = \partial_{\bar{t}}\mathrm{v} - \frac{\bar{R}\partial_{\bar{t}} s}{1+s}\partial_{\bar{R}}\mathrm{v},
\end{aligned} \tag{6}$$

and similar more complex expressions for the second derivatives. The resulting lengthy transformed equations are solved numerically by use of a spectral-collocation method (Canuto, Hussaini, Quarteroni & Zang 1988), according to which the velocity vector components in spherical coordinates, pressure, and temperature are represented as series of Chebyshev polynomials $T_n(\bar{R})$ and Legendre functions $P_n(\mu)$, $P_n^1(\mu)$:

$$V_R = u = \sum_{n=1}^{N}\sum_{m=1}^{M} u_{nm1} P_{n-1}(\mu) T_{2m-2}(\bar{R}),$$

$$V_\theta = \mathrm{v} = \sum_{n=1}^{N}\sum_{m=1}^{M} u_{nm2} P_n^1(\mu) T_{2m-2}(\bar{R}), \quad (7)$$

$$p = \sum_{n=1}^{N}\sum_{m=1}^{M} u_{nm3} P_{n-1}(\mu) T_{2m-2}(\bar{R}),$$

$$T = \sum_{n=1}^{N}\sum_{m=1}^{M} T_{nm} P_{n-1}(\mu) T_{2m-2}(\bar{R}), \quad (8)$$

and the deformed external boundary is given by $R = R_0(1 + s(\mu))$, $\bar{R} = 1$. The equations (1)-(5) are discretised on the grid:

- extrema and endpoints for T_{2M-2}:

$$\bar{R}_i = \cos[\tfrac{\pi}{2}(1 - \frac{i-1}{M-1})] \in [0,1]\ ;\ i = 1,2,\ldots M$$

- P_{N-2} (μ) extrema and endpoints which are computed numerically.

For the Navier-Stokes equations a second order fully implicit time discretization and iterative linearisation for non-linear terms is implemented according to the following scheme:

$$\begin{aligned} &\frac{3\mathbf{v}^k - 4\mathbf{v}^{k-1} + \mathbf{v}^{k-2}}{2\Delta t} \\ &-\tfrac{1}{2}\mathbf{v}^k \times \mathbf{w}^{k-1/2} - \tfrac{1}{2}\mathbf{v}^{k-1/2} \times \mathbf{w}^k = \\ &-\nabla(\rho^{-1} p^k + \tfrac{1}{2}\mathbf{v}^k \mathbf{v}^{k-1/2}) + \nabla\cdot(\nu_e^{k-1}(\nabla \mathbf{v}^k + \nabla \mathbf{v}^{k*}) \\ &-K_D \mathbf{v}^k + \rho^{-1}\mathbf{j}^{k-1} \times \mathbf{B}^{k-1} + \mathbf{g}, \end{aligned} \quad (9)$$

iterations over non-linear terms are performed at each time step until $\left\|\vec{\mathrm{u}}^{\mathrm{k}} - \vec{\mathrm{u}}^{\mathrm{k-1/2}}\right\| < \varepsilon$, typically 2-4 iterations are necessary. Occasionally the first order Euler scheme is applied when the iterations are not converging (to reduce the time step) or when the solution is sufficiently smooth to increase the time step. A similar scheme is used to advance the free surface function $s(\mu, t)$ according to (3). The procedure is stable for typical time steps Δt=5ms.

The electromagnetic force is recalculated at each time step according to the following procedure implemented with the same grid as the fluid dynamic equations, that ensures a high resolution within the external boundary layer because of the dense Chebyshev grid in this region. The metal charge is surrounded by a coaxial coil carrying a given AC electric current (fixed current power source). We are interested in the electric current and magnetic field distributions within the metal, which in the axisymmetric situation are described by means of vector potential azimuthal component A_φ (R, Θ, t) related to the magnetic field as $\mathbf{B} = \nabla \times \mathbf{A}$. In the AC case all functions can be expressed by means of complex exponents for time dependence: $Q(x,t) = \mathrm{Re}[Q(x)e^{iwt}]$. Then the electric current is given by Ohm's law: $\mathbf{J} = -i\omega\sigma\mathbf{A}$ and the Ampere's law gives the equation to determine the vector potential:

$$\nabla^2 \mathbf{A} = -i\omega\mu\sigma\mathbf{A}, \quad (10)$$

which is solved by dividing the conducting region in rings according to the prescribed grid. Then the solution can be represented analytically as a superposition of the rings' mutual inductances $\mathrm{M}(\mathrm{R_i}, Z_j; R_m, Z_n)$, self inductances and the source coil contributions $M_s(\mathrm{R_i}, Z_j; R_s, Z_s)$ which can all be expressed by means of elliptic integrals (Smythe 1989). Finally we have the set of algebraic equations to solve:

$$\mathrm{A}_\varphi(\mathrm{R_i}, \mathrm{Z_j}) = \sum_{m,n} \mathrm{M}(\mathrm{R_i}, Z_j; R_m, Z_n)\ A_\varphi(R_m, Z_n) + \sum_s M_s(\mathrm{R_i}, Z_j; R_s, Z_s) I_s(R_s, Z_s) \quad (11)$$

The magnetic field can be expressed analytically in terms of elliptic integrals without the need for numerical differentiation:

$$\mathrm{B_{R/Z}}(\mathrm{R_i}, \mathrm{Z_j}) = \sum_{m,n} \mathrm{G_{R/Z}}(\mathrm{R_i}, \mathrm{Z_j}; \mathrm{R_m}, \mathrm{Z_n}) \mathrm{A_j}(\mathrm{R_m}, \mathrm{Z_n}) + \sum_{m,n} \mathrm{G^s_{R/Z}}(\mathrm{R_i}, \mathrm{Z_j}; \mathrm{R_s}, \mathrm{Z_s}) \mathrm{I_s}(\mathrm{R_s}, \mathrm{Z_s}) \quad (12)$$

and the time average values for electromagnetic force and Joule heating can then be calculated and used as source terms in the momentum and heat equations respectively.

RESULTS

The calculated results are presented for the case of geometrical configurations and material parameters for pure Al given in (Bhamidipati,1995), including temperature dependence for electrical conductivity and the heat transfer coefficient. The numerical solution was tested by varying the grid, by the total volume and integral momentum conservation rules. A typical calculation used a grid with M=16, N=24. The electromagnetic equations (11) were solved on the double grid, N=48, to obtain a better resolution for the internal electromagnetic field, which was validated against the analytical solution for the case of a conducting sphere surrounded by a current filament ring (Smythe 1989). The comparison with the analytical solution showed the importance of self-inductance and a proper spatial resolution in simulating such details of the electromagnetic field distribution as a region of oppositely directed electric current further inwards from the high density current in the boundary layer (Fig.1) and the smoothness of the tangential magnetic field within the skin-layer (Fig.2).

The present test calculation for temperature field was started at room temperature letting, the solid cylinder to be heated by Joule heat with the coil being located stationary as shown in the Figures. The heating stage was run with large time steps (10 s) until after 540 s an excess of 20° over the Al melting temperature T=660° was reached. At this time moment the hydrodynamics simulation was started. (There is no principal difficulty to follow the motion of the coil coupled to the melt front position at earlier stages, yet it would take much longer computationally.) The present simulation run took 48 hours on Sun-Sparc 20 computer, to perform 300 time steps.

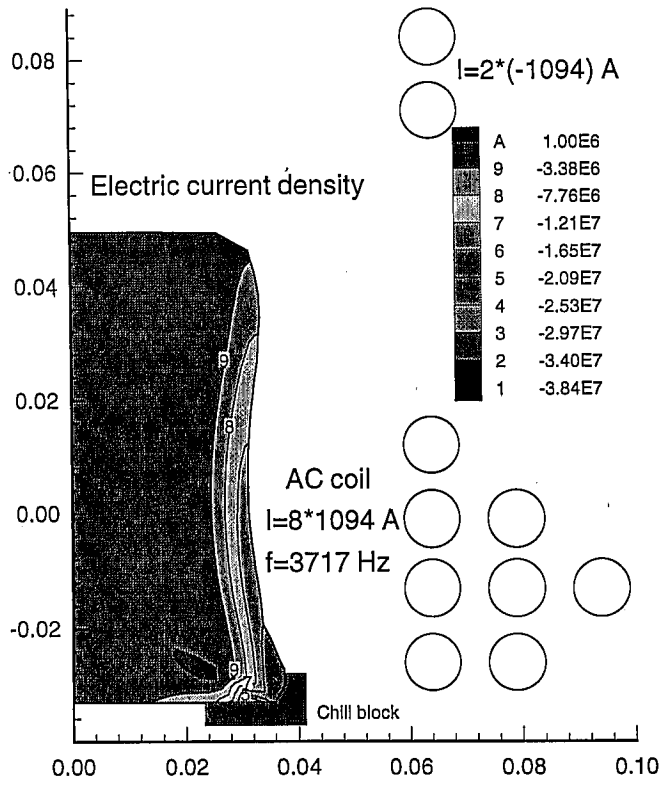

Fig.1. Computed electric current density distribution within the melted Al.

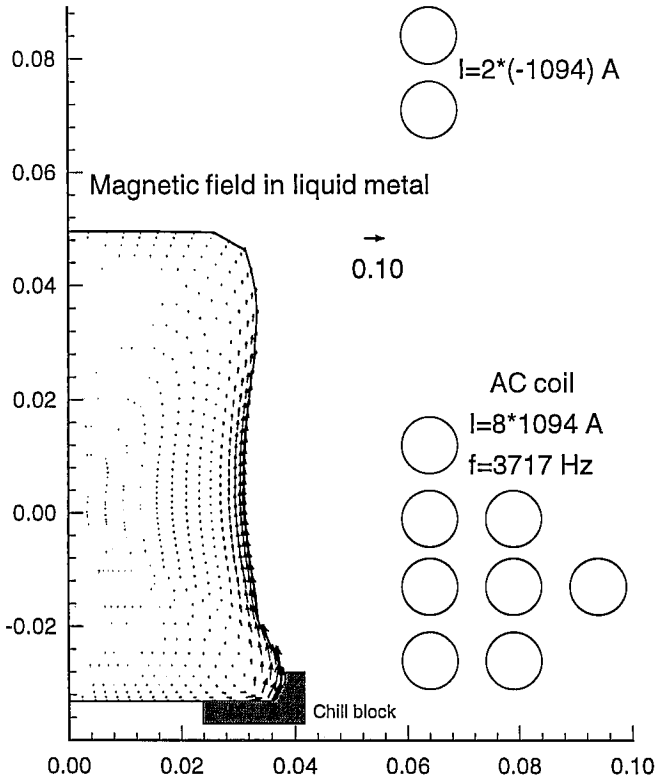

Fig.2. Calculated magnetic field and the coil configuration in the semi-levitation process (cross-section in a meridional plane).

Initially the flow field is dominated by the liquid metal shape changes under the action of the electromagnetic compression force (Fig.3). The largest velocities being observed near the symmetry axis. The top part of the free surface develops in a convex shape which at later stages changes to a concave. For some coil designs this process, according to our test simulations, leads to an intense wave motion at the free surface of liquid metal. The present configuration was found to be relatively stable with very little oscillation of the free surface.

The isotherm 4 marks the melting front which is moving during the course of flow development and continued Joule heating (Figs.3-5). It is remarkable that the liquid zone first reaches the edge of the chill block with the central region still being solid; this can be explained by the Joule heating being the most intense near the lower corner of the melted metal region where the highest current density is induced (compare to Fig. 1). In addition to this effect, an intense flow is developing at later stages in the vicinity of the lower corner, that affects the melting front motion owing to convective effects (Figs. 4-5).

At the later stages of the flow development a shear layer is observed near the side free surface where the downward flow has no resistance owing to the free slip boundary condition (3). An indication of rotating, oscillating, smaller scale vortices can be seen in the images of the developed flow (Fig. 5), however, this effect should be checked with a higher resolution runs. The most intense flow is observed in the closed vortex which is created at the lower corner in the direct vicinity of the source coil.

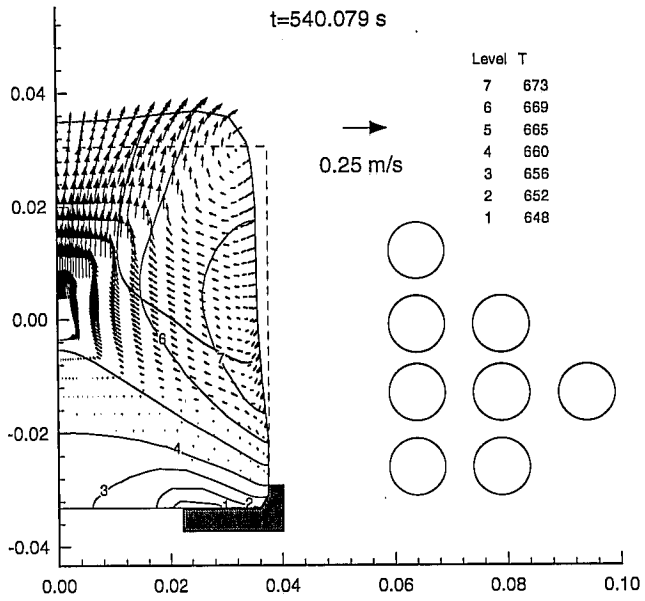

Fig.3. Initial velocity and temperature fields (after 27 fluid flow time steps) shortly after the flow initialisation at t=540s (54 temperature steps).

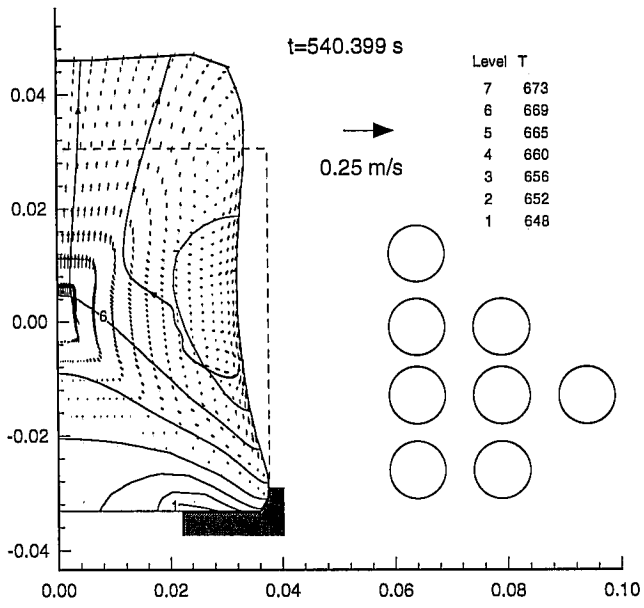

Fig.4. Velocity and temperature fields at an intermediate stage of flow and liquid metal boundary development (118 flow time steps).

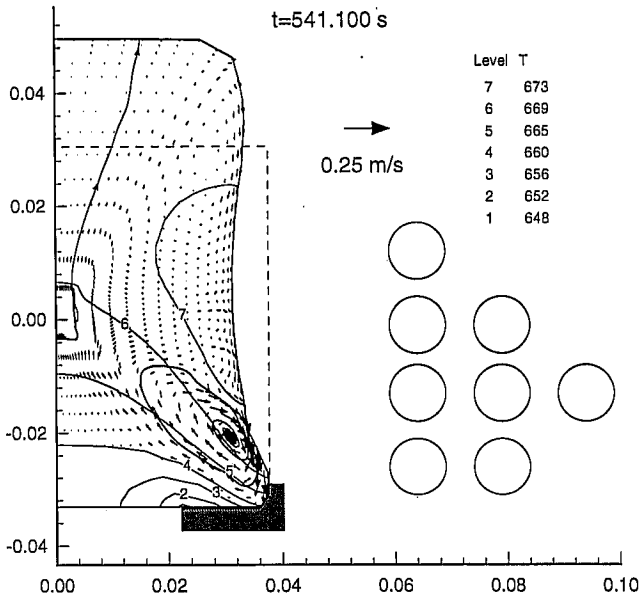

Fig 5. Velocity and temperature fields at a final stage of flow and liquid metal boundary development (270 flow time steps).

CONCLUSIONS

This work attempts to introduce a truly dynamic model of the magnetic semi-levitation process. The assumptions of "magnetic pressure", fixing quasi-static surface profile and top surface profile avoided, to enable true dynamic evolution of the process. The resulting CFD model incorporates several novel items, including an accurate electric current density calculation and a suitable turbulence model. The simulations show a detailed and complex nature of the highly coupled and non-linear flow-heat-electromagnetic fields interaction.The model was validated against analytical electromagnetic solutions, integral volume and momentum conservation laws. Peculiar features of different coil designs were found during test simulations. The code is sufficiently universal allowing to adapt it to other axisymmetric applications of electromagnetic material processing.

REFERENCES

1. J.R.Bhamidipati, N.El-Kaddah (1991). Calculation of Electromagnetic Field and Melt Shape in the Magnetic Suspension Melting Process. In "MHD in Process Metallurgy" ed. J.Szekely et al., Minerals, Metals&Materials Society, pp.69-74.
2. J.R.Bhamidipati (1995). Mathematical Modelling of Electromagnetic Field, Free Surface, Heat Transfer, and Fluid Flow Phenomena in Electromagnetic Confinement Systems. Ph.D.Thesis, University of Alabama, 138 pp.
3. A.D.Sneyd and H.K.Moffatt (1982). Fluid Dynamical Aspects of the Levitation-Melting Process. J.Fluid Mech., vol. 117, 45-70.
4. A.J.Mestel (1982). Magnetic Levitation of Liquid Metals. J.Fluid Mech., vol.117, 27-43.
5. C.Canuto, M.Y.Hussaini, A.Quarteroni, T.A.Zang (1988). Spectral Methods in Fluid Dynamics. Springer, Berlin. 567 pp.
6. W.R.Smythe (1989). Static and Dynamic Electricity. Hemisphere, New-York.